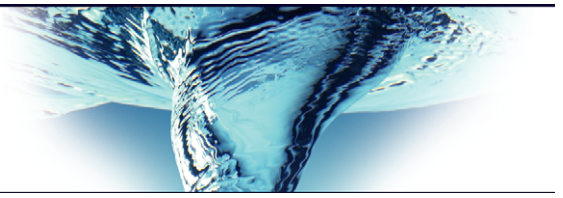
JFM RAPIDS
journals.cambridge.org/rapids



Stabilization of a swept-wing boundary layer by distributed roughness elements

Seyed M. Hosseini[1], David Tempelmann[1], Ardeshir Hanifi[1,2],† and Dan S. Henningson[1]

[1]Department of Mechanics, Linné Flow Centre, KTH Royal Institute of Technology, SeRC, SE-100 44 Stockholm, Sweden

[2]Swedish Defense Research Agency, FOI, SE-164 90 Stockholm, Sweden

(Received 7 September 2012; revised 21 November 2012; accepted 10 January 2013; first published online 8 February 2013)

The stabilization of a swept-wing boundary layer by distributed surface roughness elements is studied by performing direct numerical simulations. The configuration resembles experiments studied by Saric and coworkers at Arizona State University, who employed this control method in order to delay transition. An array of cylindrical roughness elements are placed near the leading edge to excite subcritical cross-flow modes. Subcritical refers to the modes that are not critical with respect to transition. Their amplification to nonlinear amplitudes modifies the base flow such that the most unstable cross-flow mode and secondary instabilities are damped, resulting in downstream shift of the transition location. The experiments by Saric and coworkers were performed at low levels of free stream turbulence, and the boundary layer was therefore dominated by stationary cross-flow disturbances. Here, we consider a more complex disturbance field, which comprises both steady and unsteady instabilities of similar amplitudes. It is demonstrated that the control is robust with respect to complex disturbance fields as transition is shifted from 45 to 65 % chord.

Key words: boundary layer receptivity, flow control, transition to turbulence

1. Introduction

The three-dimensional nature of boundary layers on aircraft carries miscellaneous intrinsic instabilities. One characteristic instability is the so-called cross-flow instability, which is due to an inflection point in the cross-flow component of the velocity profile. This instability generates streamwise vortices, which can appear in the form of stationary and non-stationary disturbances, where the latter is common in environments with high external disturbance (cf. the reviews by Bippes 1999; Saric, Reed & White 2003). Depending on the flow regime, such disturbances grow and cause transition,

† Email address for correspondence: ardeshir.hanifi@foi.se

doi:10.1017/jfm.2013.33

https://doi.org/10.1017/jfm.2013.33 Published online by Cambridge University Press

yielding a turbulent boundary layer with a higher friction coefficient. Numerous methods have been introduced in order to control such instabilities.

One such control mechanism was initially proposed and successfully employed by Saric, Carillo & Reibert (1998). One spanwise row of uniformly distributed cylindrical roughness elements of micron-sized height localized in the streamwise direction were used to excite subcritical cross-flow disturbances. Compared to the most unstable disturbances, the latter were chosen to have relatively short wavelengths. Saric *et al.* (1998) chose 2/3 of the wavelength of the naturally most unstable cross-flow mode. Such high-wavenumber disturbances grow strongly in regions close to the leading edge but decay farther downstream in appropriate base flows. Hence, the excitation of these modes provides a means to distort the mean flow in a way that favourably affects the evolution of the naturally most unstable instability. Under 'natural' conditions, in a low-turbulence environment, the transition location could be shifted from 71 % chord to nearly 80 % chord, which is downstream of the pressure minimum of the used wing at negative angles of attack. By solving the nonlinear parabolized stability equations (NPSEs), Malik *et al.* (1999) confirmed the stabilizing effect of subcritical disturbances for the same flow configuration. Recently, free-flight experiments have been performed by Carpenter, Saric & Reed (2008), showing that control by surface roughness is also efficient at higher realistic Reynolds numbers. Also, for this configuration, NPSE solutions confirmed the experimental observations (cf. Li *et al.* 2009).

A comprehensive numerical study was performed by Wassermann & Kloker (2002). Employing direct numerical simulations (DNSs), they studied the transition and stabilization of a three-dimensional flat-plate boundary layer, which was dominated by steady primary cross-flow disturbances. These authors show that the 'control' mode nonlinearly affects the mean flow in a similar manner as does suction at the wall. By comparison with the undisturbed base flow, they observed a reduced cross-flow, while the streamwise profiles became fuller in the near-wall region. By performing stability computations employing the distorted mean flow, they showed that the mean flow modification on its own can be attributed to a significant stabilization of the most unstable cross-flow disturbances. Further, Wassermann & Kloker (2002) observed the control mode to decrease nonlinearly regions of deceleration of the steady three-dimensional flow state. The latter arises due to the streaky nature of stationary cross-flow disturbances, which cause a strong mean flow distortion in the uncontrolled case. Since a strong deceleration favours the growth of secondary instabilities, Wassermann & Kloker (2002) concluded that the control not only stabilizes the primary cross-flow modes but also attenuates the growth of secondary instabilities.

In this paper we study the stabilization of a swept-wing boundary layer by means of DNSs. Transition control is achieved by distributed cylindrical roughness elements spaced such as to excite cross-flow modes, which are subcritical with respect to transition. First we study effects of the control on the mean flow as well as the steady primary cross-flow modes. The flow configuration resembles experiments by Saric *et al.* (1998); however, we disregard any unsteady disturbances due to the high spectral accuracy of the code and thus do not obtain transition. In a second set of DNSs we move closer towards real experiments and introduce unsteady disturbances by a random volume force. However, we consider a boundary layer where both steady and unsteady cross-flow modes coexist and are of similar amplitudes. Hence, the case studied here is more complex than the configurations considered in previous studies

https://doi.org/10.1017/jfm.2013.33 Published online by Cambridge University Press

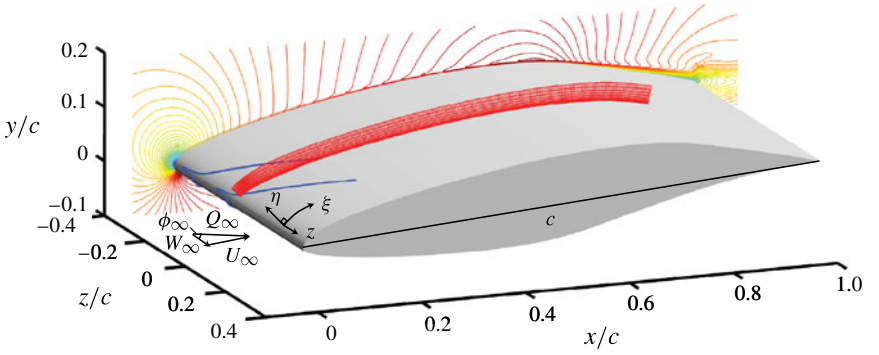


FIGURE 1. Swept NLF(2)-415 wing, with sweep angle ϕ_∞ and the total incoming velocity Q_∞. The wing is at an angle of attack of $-4°$. Here (ξ, η, z) and (x, y, z) represent locally fitted curvilinear and Cartesian coordinate systems, respectively; and (u_ξ, v_η, w) and (u, v, w) are the corresponding defined velocities in the introduced coordinate systems. The spectral elements for DNS are depicted in red. The normalized streamwise velocity contour lines from the RANS solution are shown ranging from 0.0 to 1.54, with a spacing of 0.024, values that are used for the DNS base flow. The blue lines represent the streamlines of the base flow.

on stabilization and would correspond to experiments performed in a wind tunnel that exhibits higher levels of free stream turbulence as compared with the one used by Saric *et al.* (1998). This allows us to evaluate the robustness of the control approach.

2. Flow configuration

We examine disturbance evolution and control of the boundary layer flow over a swept wing (NLF(2)-0415; Somers & Horstmann 1985) mounted in a wind tunnel at an angle of attack of $\alpha = -4°$. Note that α is defined in a plane normal to the leading edge. The sweep angle is $\phi_\infty = 45°$. The wing geometry is invariant in the spanwise direction. This configuration favours the growth of cross-flow disturbances because of a strong favourable pressure gradient on the upper wing side. The chord Reynolds number considered is $Re_C = Q_\infty C/\nu = 2.4 \times 10^6$, which is based on the long swept chord, i.e. $C = c/\cos(\phi) = 1.83$ m, while c, the unswept short chord, is defined in figure 1. The total incoming free stream velocity is represented by $Q_\infty = 18.5$ m s^{-1}, and ν is the kinematic viscosity.

This flow configuration conforms to the experiments by Saric *et al.* (1998), who excited cross-flow disturbances that were aimed at nonlinearly stabilizing the boundary layer. These were generated in a controlled manner by placing a spanwise array of micron-sized roughness elements close to the leading edge. The roughness elements were placed at $x/c = 0.023$ with a spacing $L_z = 8$ mm, where x denotes the chordwise direction (see figure 1). The wavelength of the naturally most unstable stationary cross-flow mode is $\lambda_z = 12$ mm. Hence, the wavelength of the 'control' mode excited by the roughness cylinders corresponds to 2/3 of the wavelength of the most unstable mode. The height and diameter of the elements were chosen as $\varepsilon_r = 6$ μm and $d_r = 2$ mm, respectively.

https://doi.org/10.1017/jfm.2013.33 Published online by Cambridge University Press

3. Direct numerical simulations

Direct numerical simulations were performed using the incompressible solver 'Nek5000' by Fischer, Lottes & Kerkemeier (2008), which builds on the spectral element method (SEM). The latter was originally introduced by Patera (1984) and combines the geometrical flexibility of finite element methods with the accuracy provided by spectral methods. The spatial discretization is obtained by decomposing the physical domain into spectral elements. The solution to the Navier–Stokes equations is approximated element-wise as a sum of Lagrange interpolants defined by an orthogonal basis of Legendre polynomials up to degree N. The following results have been obtained using $N = 11$. The present SEM code is optimized for MPI-based (Message Passing Interface) usage on supercomputers with thousands of processors (Tufo & Fischer 2001). Here, we have performed parallel computations on 4104 processors.

Despite the parallel efficiency of the code, a DNS of the whole wind tunnel test section is still unfeasible. In order to reduce the computational cost, we make use of previous DNS solutions by Tempelmann *et al.* (2012), who computed a steady base flow for a domain extending from $x/c = 0.04$ on the lower wing side to $x/c = 0.7$ on the upper wing side and thus accounted for the asymmetry of the configuration. That solution was obtained by prescribing Dirichlet boundary conditions at the free stream boundaries, which were extracted from complementary Reynolds-averaged Navier–Stokes (RANS) computations.

Here, in turn, we choose the computational domain to be entirely located on the upper wing side (cf. figure 1) and prescribe Dirichlet conditions at the inflow ($x/c = 0.01$) and free stream boundaries, respectively. The corresponding velocities are extracted from the steady base flow computed by RANS, which is obtained by manually prescribing the transition location at $x/c \approx 0.7$ on the upper side and $x/c \approx 0.01$ on the lower side. Further, we choose zero-slip conditions at the wall while zero-stress boundary conditions are imposed at the outflow of the domain ($x/c = 0.8$). Periodic boundary conditions are prescribed at the lateral boundaries. The width of the domain is chosen such that both the control mode as well as the naturally most unstable cross-flow disturbance can be accounted for, i.e. it corresponds to 24 mm. The numerical grid consists of 54 450 spectral elements and is shown in figure 1. It has been generated using the gridgen-c code by Sakov (2011).

A total of 18 elements have been used to discretize the spanwise direction. At the outflow of the computational domain for $x/c > 0.78$, we use a sponge region similar to the one used by Tempelmann *et al.* (2012), which forces the DNS solution to that of the undisturbed boundary layer. However, here it is used to avoid reflections as well as possible back flow because of separation at the outflow boundary. Note that in the case of separation the base flow is ramped to the time-averaged solution of the separation bubble.

3.1. *Stationary perturbations*

The control mode was excited by circular cylinders, while multiple steady cross-flow modes including the naturally most unstable mode emerged because of the presence of natural surface roughness in the leading edge region. The wing model employed for the experiments was hand polished, exhibiting a root mean square (r.m.s.) natural roughness height of the order of 0.25 μm (cf. Reibert *et al.* 1996). Here, we have to model both the excitation of stationary cross-flow disturbances by natural roughness and the control cylinders stimulating the cross-flow mode, which is aimed at damping

https://doi.org/10.1017/jfm.2013.33 Published online by Cambridge University Press

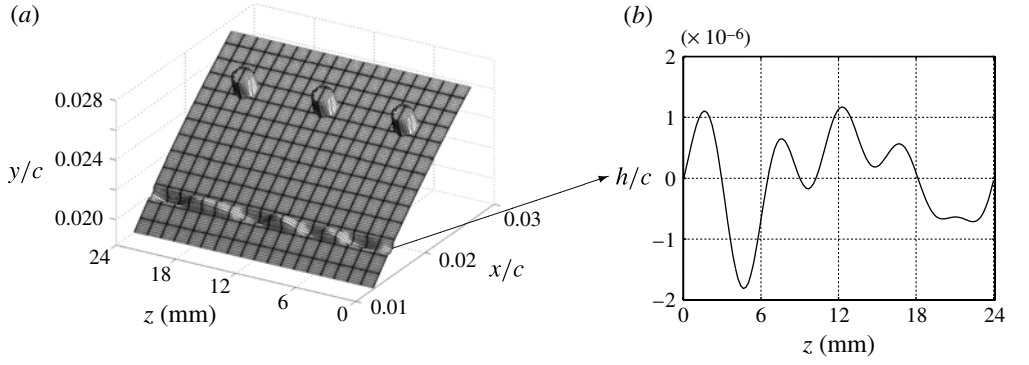


FIGURE 2. (*a*) Visualization of both the 'natural' surface roughness (modelled) and the circular roughness cylinders (meshed). The amplitudes are exaggerated for visualization purposes. (*b*) Amplitude of the 'natural' roughness in physical space at $x/c = 0.015$.

the most unstable stationary cross-flow mode. The set-up of the DNS is very similar to the one by Tempelmann *et al.* (2012), who predicted receptivity amplitudes that were ∼2.6 times lower as compared with the experiments by Reibert *et al.* (1996). These in turn were similar to the control experiments by Saric *et al.* (1998). Hence, in order to obtain a flow that is comparable to the experimental boundary layer, we choose roughness heights that are 2.6 times higher than those used in the experiments. Note that this is still in the linear regime of receptivity (cf. Tempelmann *et al.* 2012).

The excitation of multiple stationary cross-flow disturbances is modelled in a very simplified manner. The domain width chosen dictates the wavelength of the fundamental mode. Here, the latter has a spanwise wavenumber $\beta_0 = 2\pi/\lambda_z$ with $\lambda_z = 24$ mm. Because of periodic boundary conditions, only disturbances with wavenumbers $n\beta_0$ can be accounted for in the DNS while $n = 1, 2, \ldots, N$. Complementary linear parabolized stability equation (PSE) computations revealed that only stationary cross-flow modes with $n = 1, 2, \ldots, 5$ grow significantly. The excitation of these is therefore modelled by inserting a roughness strip of the form $h(x, z) = \epsilon_r H_\beta(x) \sum_{n=1}^{5} \sin(n\beta_0 z + \varphi_n)$, where h denotes displacement in the wall-normal direction. The height of the roughness elements ϵ_r is chosen such as to obtain the desired r.m.s. value of $\epsilon_r = 2.6 \times 0.25\ \mu\text{m} = 0.65\ \mu\text{m}$. The roughness shape is defined as $H_\beta(x) = [S((x - h_s)/h_r) - S((x - h_e)/h_f + 1)]$, with S being a smooth step function defined in Schrader, Brandt & Henningson (2009). Here we choose $h_s/c = 0.014$, $h_e/c = 0.015$, $h_r/c = h_f/c = 2.75 \times 10^{-4}$, yielding a roughness position of $x/c = 0.015$. The phase of each mode denoted by φ_n is chosen randomly. The resulting surface roughness is visualized in figure 2. Note that this roughness is modelled by inhomogeneous boundary conditions and referred to in this paper as 'natural' surface roughness. We thus project the zero-slip condition on the surface of the roughness to the smooth undisturbed wall. The cylindrical roughness elements used to excite the control mode, on the other hand, are inserted into the computational grid by displacing the respective Gauss–Lobatto–Legendre (GLL) points at the wall. Their chordwise position is chosen as $x_r/c = 0.023$, i.e. close to the experimental position, while the height is $\varepsilon = 2.6 \times 6\ \mu\text{m} = 15.6\ \mu\text{m}$. Also these elements are shown in figure 2.

https://doi.org/10.1017/jfm.2013.33 Published online by Cambridge University Press

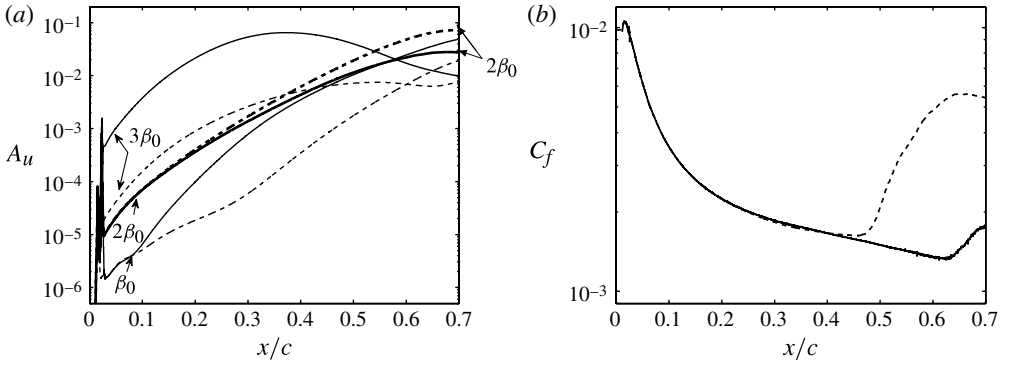


FIGURE 3. (*a*) The amplitude A_u of the stationary modes for both the natural (– – –) and the controlled (——) cases in the absence of unsteady perturbations; and (*b*) the time-averaged friction coefficient for the natural (– – –) and the controlled (——) cases in the presence of unsteady perturbations.

3.2. *Non-stationary perturbations*

The growth of unsteady instabilities, both primary and secondary, and the subsequent breakdown to turbulent flow requires the presence of ambient unsteady disturbances such as acoustic noise or free stream turbulence. In this study we choose to artificially introduce non-stationary disturbances inside the boundary layer by employing a weak randomly pulsed volume force. Its specific form is given in Högberg & Henningson (1998). The forcing is directed normal to the wall and located at $x_r/c = 0.017$.

The amplitude of the forcing is chosen such that transition is obtained at ∼45 % chord in the presence of active roughness strip, which is significantly upstream of the transition location observed in the experiments by Saric *et al.* (1998). This choice allows us to reduce the computational cost, as we can study transition control within a shorter computational box while assuring that the sponge region at the outflow does not affect our results. Further, this choice leads to the emergence of primary travelling cross-flow disturbances of higher amplitude as compared with the experiments by Saric *et al.* (1998). Hence, the transition scenario will not be dominated by stationary disturbances only, but by both unsteady and steady primary instabilities. While this certainly complicates the identification of physical mechanisms, it allows the evaluation of the robustness of the control with respect to rather complex disturbance environments.

4. Stabilization of primary disturbances and transition control

We start our investigation on subcritical roughness control by studying its effect on primary steady cross-flow disturbances. Two cases are considered. First we disturb the boundary layer using the natural roughness model only. A second DNS is then performed comprising both the natural and the control roughness. In the following these cases are denoted the ‘natural’ and the ‘controlled’ case, respectively. Figure 3(*a*) shows the amplitudes of the stationary modes $A_u = \max_\eta(|\hat{u}_\xi|/\bar{U}_{\xi,e})$, for the two cases, where a hat denotes a spatial r.m.s. amplitude with respect to z of the individual modal disturbances and $\bar{U}_{\xi,e}$ represents the boundary layer edge velocity. It is apparent that the 12 mm mode ($2\beta_0$) grows continuously through the domain and becomes

https://doi.org/10.1017/jfm.2013.33 Published online by Cambridge University Press

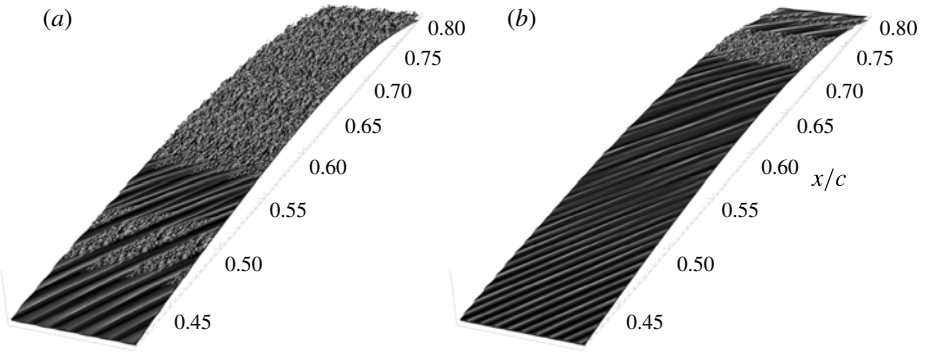


FIGURE 4. Isosurfaces of the instantaneous velocity U. Three fundamental spanwise periods are shown for visualization purposes. (a) Natural case; (b) controlled case.

dominant after $x/c = 0.3$. The other modes also grow initially, but the growth of $(3\beta_0)$ becomes weaker downstream. In the controlled scenario, the control mode (i.e. $\beta = 3\beta_0$) exhibits strong initial growth, but decays further downstream. The additional cases comprising flow transition correlate this behaviour with transition location. Complementary PSE simulations are also presented in Tempelmann (2011) to rule out any grid dependence.

Because of the high accuracy of the DNS code, additional unsteady perturbations are added to the previous cases in order to obtain transition. Figure 3(b) shows the computed time-averaged friction coefficient ($C_f = 2\mu(\partial u/\partial\eta)/(\rho U_{\xi,e}^2)$) of the cases where transition was acquired. The time averaging was required because of the unsteadiness of the transition location for both cases ($\pm 0.05x/c$). The flow reaches transition at $x/c \approx 0.45$ in the natural case. Applying the control roughness elements efficiently delays transition well downstream despite the high levels of background noise, which can be confirmed visually by the instantaneous streamwise velocities of the two cases depicted in figures 4(a) and 4(b). This also corresponds to the experimental observations by Reibert *et al.* (1996) and Saric *et al.* (1998), where the damping of the most unstable stationary cross-flow mode is believed to have delayed transition. Similar observations were reported by Wassermann & Kloker (2002), where the modification of the mean flow resulted in the damping of this mode, leading to transition delay. These observations clearly demonstrate the robustness of the proposed method. Qualitatively, the studied cases conform to the experimental observation by Saric *et al.* (1998), who found the transition location to be shifted from $x/c = 0.71$ in the natural case to $x/c = 0.8$. Here we show that the control is able to delay transition for even higher levels of unsteady disturbances.

5. Unsteady disturbances and secondary instabilities

In order to characterize the disturbance environment and with it the transition scenario of the above described cases, the total disturbance field is decomposed into time-periodic Fourier modes. This allows us to compare the evolution of both steady and unsteady disturbances quantitatively. Furthermore, we look for those characteristic secondary instabilities that have been identified in previous studies

https://doi.org/10.1017/jfm.2013.33 Published online by Cambridge University Press

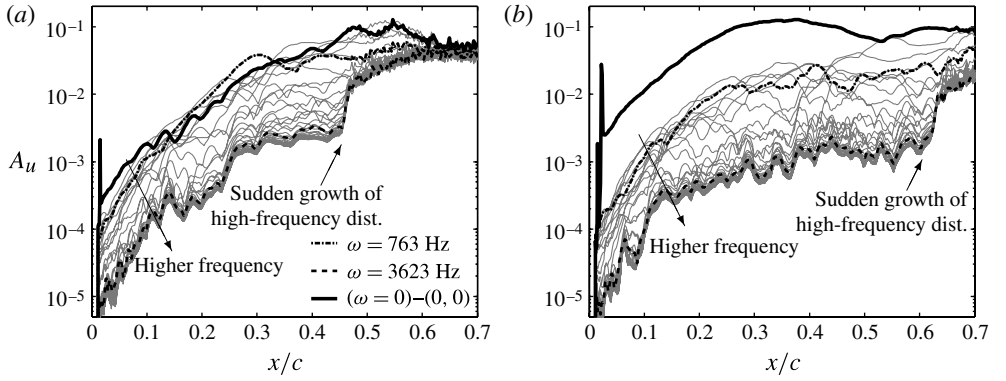


FIGURE 5. Amplitude evolution of steady and unsteady disturbances for (*a*) the natural case and (*b*) the controlled case. The grey lines represent unsteady disturbances plotted at a constant frequency step size (190 Hz).

(cf. Högberg & Henningson 1998; Malik *et al.* 1999; Wassermann & Kloker 2002, 2003). Since secondary instabilities are characterized by their two-dimensional eigenfunction nature, time-periodic Fourier modes are computed by performing fast Fourier transforms (FFTs) for several (η, z) planes distributed along the chord, i.e. $u'_\xi(\xi, \eta, z, t) = \sum_n^N \tilde{u}_\xi(\xi, \eta, z, n\omega_0)\mathrm{e}^{\mathrm{i}n\omega_0 t}$. The amplitudes of individual modes are presented in figure 5 as $A_u(x) = \max_{\eta,z}(|\tilde{u}_\xi|/\bar{U}_{\xi,e})$, for both the natural and the controlled case. Here, $\bar{U}_\xi$ denotes the spatio-temporal mean of U_ξ. The amplitudes of the steady disturbances are obtained by subtracting the mean flow, i.e. the $(0, 0)$ mode, from the zero-frequency mode $\tilde{u}_\xi(n = 0)$.

A rather complex disturbance environment becomes apparent in figure 5(*a*), where the natural case is presented. Both steady and unsteady disturbances are present and grow almost within the entire domain. The low-frequency disturbances (e.g. $\omega = 763$ Hz) are found to be of similar order as the steady disturbances in the uncontrolled case or even to exhibit higher amplitudes. Complementary linear PSE computations for the current flow configuration reveal that the most unstable cross-flow disturbances exhibit frequencies $\omega \approx 750$ Hz and spanwise wavelengths $\beta \approx 12$ mm. Hence, the low-frequency disturbances can be associated with unsteady primary cross-flow disturbances. However, also high-frequency disturbances are found to grow already far upstream of the transition location, which is at $x/c = 0.45$. This growth might be explained by the onset of early nonlinear effects, which force the high-frequency disturbances. For $x/c > 0.4$ an indication for the amplification of secondary instabilities is observed. At the position marked in figure 5(*a*), which is located just upstream of transition, high-frequency disturbances undergo sudden amplification and finally attain amplitudes that are of similar order as compared with the steady and low-frequency instabilities. This is consistent with experimental observations (cf. Deyhle & Bippes 1996; White & Saric 2005) as well as theoretical and numerical studies (Malik *et al.* 1999; Wassermann & Kloker 2002, 2003) and points to the emergence of secondary instabilities. The situation is different in the controlled case. The respective amplitudes are depicted in figure 5(*b*). The steady disturbances are clearly dominant. Their initial spatial evolution corresponds well to that of the control mode studied in § 4. Hence, the control mode excited by the circular roughness cylinders seems to

https://doi.org/10.1017/jfm.2013.33 Published online by Cambridge University Press

dominate the disturbance field for $x/c < 0.5$. It is apparent that those low-frequency disturbances which are dominant in the natural case are attenuated.

Furthermore, the sudden growth of high-frequency disturbances prior to transition is shifted downstream, corresponding to the transition location for the controlled case. The control has successfully weakened the growth of secondary instabilities. This observation confirms results by Wassermann & Kloker (2002), who found that this kind of control leads to a three-dimensional flow state that attenuates the growth of high-frequency secondary instabilities. In particular, they found the control mode to decrease regions of deceleration of the steady flow nonlinearly. A strong region of deceleration is known to favour the growth of secondary instabilities.

Because of the complex disturbance field inside the boundary layer, it is not straightforward to isolate and identify characteristic secondary instabilities. The previous investigations (by e.g. Högberg & Henningson 1998; Malik *et al.* 1999; Wassermann & Kloker 2002, 2003) were all performed under specific conditions. Boundary layer transition was induced either by stationary cross-flow disturbances or by selected travelling cross-flow instabilities. Such controlled conditions make it possible to correlate the location of secondary instabilities to certain regions of the underlying three-dimensional flow, which is characterized by saturated primary cross-flow disturbances. For example, in boundary layers where transition is induced by stationary cross-flow disturbances, high-frequency secondary instabilities are associated with either the minimum spanwise gradient of the streamwise velocity ('z' mode) or the respective maximum wall-normal gradient ('y' mode). In a boundary layer that was dominated by a travelling primary cross-flow instability, Wassermann & Kloker (2003) identified similar modes. These were computed by performing a temporal Fourier transformation in a reference system, which was moving with the primary unsteady cross-flow instability.

In our case, no primary cross-flow disturbances exist for $\omega > 2000$ Hz. The high-frequency Fourier modes that have been found to experience sudden growth prior to transition are thus solely associated with unstable secondary instabilities. The two-dimensional amplitude distribution $\tilde{u}(\eta, z)$ of a characteristic high-frequency mode with $\omega = 3622$ Hz is shown in figure 6 for both the natural and the controlled cases. Additionally, contour lines of the underlying instantaneous total velocity field are shown, which is characterized by the vortical structure of a dominant unsteady primary cross-flow mode with $\lambda_z \approx 12$ mm. The structures that become apparent in the natural case are reminiscent of a 'z' mode. The maximum amplitudes in the wall-normal plane are located in regions of strong shear at the updraught side of the primary vortices. This is where the spanwise gradients become minimal. Figure 6(*b*) shows the same Fourier mode at $x/c = 0.4$ that is obtained when the control mode is excited. The amplitudes obtained are much weaker as compared with the natural case. Further, a different structure of the instantaneous flow becomes apparent, which reflects the dominance of the steady control mode. Thus the secondary instabilities have been suppressed here.

6. Conclusions and outlook

Direct numerical simulations of a swept-wing boundary layer have been performed. The flow configuration conforms to experiments conducted by Saric and coworkers at the Arizona State University (see e.g. Reibert *et al.* 1996; Saric *et al.* 1998). Transition control is achieved by placing a periodic row of circular roughness cylinders close to the leading edge. The spacing of these was chosen such as to excite primarily a

https://doi.org/10.1017/jfm.2013.33 Published online by Cambridge University Press

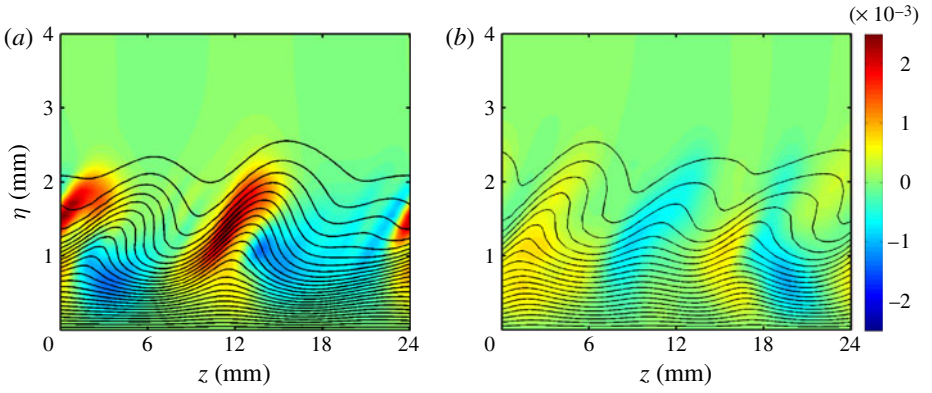


FIGURE 6. Two-dimensional amplitude distribution of a high-frequency Fourier mode with $\omega = 3622$ Hz in a wall-normal plane (η, z) at $x/c = 0.4$. Pseudocolours represent the real part of the Fourier amplitude. Contour lines denote the instantaneous flow field. (*a*) Natural case; (*b*) controlled case.

steady cross-flow disturbance that is subcritical with respect to transition. This mode experiences strong initial growth but decays farther downstream. Excitation of multiple steady cross-flow disturbances has been realized by an appropriate simplified model of natural roughness.

We have first considered the excitation of steady cross-flow instabilities only, i.e. transition is not studied. Earlier results by Saric *et al.* (1998), Malik *et al.* (1999) and Wassermann & Kloker (2002) are confirmed, as we observe the naturally most unstable steady cross-flow mode to be attenuated by the control because of a nonlinearly distorted mean flow. Two additional simulations have been performed herein. A random time-dependent volume force is introduced close to the leading edge, which excites unsteady disturbances. The amplitude is adjusted ($O \approx 10^{-4}$) such as to obtain transition from laminar to turbulent flow at $x/c \approx 0.45$. Consequently, transition is not caused by breakdown of dominating stationary disturbances as in the experiments but by breakdown of coexisting steady and unsteady cross-flow disturbances, which exhibit similar amplitudes. We demonstrate that, upon exciting the steady control mode, transition is shifted downstream. It is shown that both the most unstable unsteady primary disturbances and high-frequency secondary instabilities are attenuated when control is employed.

So far the control approach studied herein has only been used for boundary layers dominated by stationary cross-flow disturbances. Here, we demonstrate that the control is robust. It effectively delays transition induced by a complex disturbance field involving both steady and unsteady primary cross-flow disturbances by suppressing the secondary instabilities.

Acknowledgements

The authors wish to thank J. Malm for implementing the random volume forcing as well as P. Schlatter and M. Kloker for fruitful discussions and valuable comments. Computer time provided by SNIC (Swedish National Infrastructure for Computing) at the Center for Parallel Computers (PDC), KTH, is gratefully acknowledged. This work

https://doi.org/10.1017/jfm.2013.33 Published online by Cambridge University Press

has been supported by the European Commission through the FP7 project 'RECEPT' (Grant Agreement no. ACPO-GA-2010-265094)

References

BIPPES, H. 1999 Basic experiments on transition in three-dimensional boundary layers dominated by cross-flow instability. *Prog. Aerosp. Sci.* **35**, 363–412.

CARPENTER, A., SARIC, W. S. & REED, H. L. 2008 Laminar flow control on a swept wing with distributed roughness. *AIAA Paper* 2008-7335.

DEYHLE, H. & BIPPES, H. 1996 Disturbance growth in an unstable three-dimensional boundary layer and its dependence on environmental conditions. *J. Fluid Mech.* **316**, 73–113.

FISCHER, P. F., LOTTES, J. W. & KERKEMEIER, S. G. 2008 nek5000 web page. http://nek5000.mcs.anl.gov.

HÖGBERG, M. & HENNINGSON, D. 1998 Secondary instability of cross-flow vortices in Falkner–Skan–Cooke boundary layers. *J. Fluid Mech.* **368**, 339–357.

LI, F., CHOUDHARI, M., CHANG, C.-L., STREETT, C. & CARPENTER, M. 2009 Roughness based cross-flow transition control: a computational assessment. *AIAA Paper* 2009-4105.

MALIK, M. R., LI, F., CHOUDHARI, M. M. & CHANG, C.-L. 1999 Secondary instability of cross-flow vortices and swept-wing boundary-layer transition. *J. Fluid Mech.* **399**, 85–115.

PATERA, A. T. 1984 A spectral element method for fluid dynamics: laminar flow in a channel expansion. *J. Comput. Phys.* **54**, 468–488.

REIBERT, M. S., SARIC, W. S., CARILLO, R. B. & CHAPMAN, K. L. 1996 Experiments in nonlinear saturation of stationary cross-flow vortices in a swept-wing boundary layer. *AIAA Paper* 96-0184.

SAKOV, P. 2011 gridgen-c – an orthogonal grid generator based on the crdt algorithm (by conformal mapping). http://code.google.com/p/gridgen-c/.

SARIC, W. S. Jr., CARILLO, R. B. & REIBERT, M. S. 1998 Leading-edge roughness as a transition control mechanism. *AIAA Paper* 98-0781.

SARIC, W. S., REED, H. L. & WHITE, E. B. 2003 Stability and transition of three-dimensional boundary layers. *Annu. Rev. Fluid Mech.* **35**, 413–440.

SCHRADER, L. U., BRANDT, L. & HENNINGSON, D. S. 2009 Receptivity mechanisms in three-dimensional boundary layer flows. *J. Fluid Mech.* **618**, 209–241.

SOMERS, D. M. & HORSTMANN, K.-H. 1985 Design of a medium-speed, natural laminar-flow airfoil for commuter aircraft applications. *Tech. Rep.* DLR-IB 129-85/26.

TEMPELMANN, D. 2011 Receptivity of cross flow-dominated boundary layers. PhD thesis, KTH, Stockholm.

TEMPELMANN, D., SCHRADER, L.-U., HANIFI, A., BRANDT, L. & HENNINGSON, D. S. 2012 Swept wing boundary-layer receptivity to localized surface roughness. *J. Fluid Mech.* **711**, 516–544.

TUFO, H. M. & FISCHER, P. F. 2001 Fast parallel direct solvers for coarse grid problems. *J. Parallel Distrib. Comput.* **61** (2), 151–177.

WASSERMANN, P. & KLOKER, M. 2002 Mechanics and passive control of cross-flow-vortex-induced transition in a three-dimensional boundary layer. *J. Fluid Mech.* **456**, 49–84.

WASSERMANN, P. & KLOKER, M. 2003 Transition mechanisms induced by travelling cross-flow vortices in a three-dimensional boundary layer. *J. Fluid Mech.* **483**, 67–89.

WHITE, E. B. & SARIC, W. S. 2005 Secondary instability of cross-flow vortices. *J. Fluid Mech.* **525**, 275–308.

https://doi.org/10.1017/jfm.2013.33 Published online by Cambridge University Press